Monthly Notices of the ROYAL ASTRONOMICAL SOCIETY

MNRAS **461,** 3153–3164 (2016) doi:10.1093/mnras/stw1438
Advance Access publication 2016 June 20

The column density distribution of hard X-ray radio galaxies

F. Panessa,[1]★ L. Bassani,[2] R. Landi,[2] A. Bazzano,[1] D. Dallacasa,[3,4] F. La Franca,[5] A. Malizia,[2] T. Venturi[4] and P. Ubertini[1]

[1]*INAF – Istituto di Astrofisica e Planetologia Spaziali di Roma (IAPS-INAF), Via del Fosso del Cavaliere 100, I-00133 Roma, Italy*
[2]*Istituto di Astrofisica Spaziale e Fisica Cosmica (IASF-INAF), Via P. Gobetti 101, I-40129 Bologna, Italy*
[3]*Dipartimento di Fisica e Astronomia, Università di Bologna, via Ranzani, 1, I-40127 Bologna, Italy*
[4]*Osservatorio di Radioastronomia (ORA-INAF), Via P. Gobetti 101, I-40129 Bologna, Italy*
[5]*Dipartimento di Matematica e Fisica, Università degli Studi Roma Tre, via della Vasca Navale 84, I-00146 Roma, Italy*

Accepted 2016 June 14. Received 2016 June 14; in original form 2016 March 21

ABSTRACT

In order to investigate the role of absorption in active galactic nuclei (AGN) with jets, we have studied the column density distribution of a hard X-ray selected sample of radio galaxies, derived from the *INTEGRAL*/Imager on Board the Integral Satellite (IBIS) and *Swift*/The Burst Alert Telescope (BAT) AGN catalogues (∼7–10 per cent of the total AGN population). The 64 radio galaxies have a typical FR II radio morphology and are characterized by high 20–100 keV luminosities (from 10^{42} to 10^{46} erg s^{-1}) and high Eddington ratios (log $L_{\rm Bol}/L_{\rm Edd}$ typically larger than ∼0.01). The observed fraction of absorbed AGN ($N_{\rm H} > 10^{22}$ cm^{-2}) is around 40 per cent among the total sample, and ∼75 per cent among type 2 AGN. The majority of obscured AGN are narrow-line objects, while unobscured AGN are broad-line objects, obeying to the zeroth-order predictions of unified models. A significant anti-correlation between the radio core dominance parameter and the X-ray column density is found. The observed fraction of Compton thick AGN is ∼2–3 per cent, in comparison with the 5–7 per cent found in radio-quiet hard X-ray selected AGN. We have estimated the absorption and Compton thick fractions in a hard X-ray sample containing both radio galaxies and non-radio galaxies and therefore affected by the same selection biases. No statistical significant difference was found in the absorption properties of radio galaxies and non-radio galaxies sample. In particular, the Compton thick objects are likely missing in both samples and the fraction of obscured radio galaxies appears to decrease with luminosity as observed in hard X-ray non-radio galaxies.

Key words: galaxies: active – galaxies: jets – galaxies: Seyfert – radio continuum: galaxies.

1 INTRODUCTION

Unification models for active galactic nuclei (AGN) hypothesize a common structure for the central engine, where the different orientation of the line of sight determines a different classification of the source (Antonucci 1993; Urry & Padovani 1995). Material accretes around a central supermassive black hole in the form of a disc, often surrounded by a corona of hot electrons responsible for the emission at high X-ray energies. At larger scales, a dusty torus obscures the inner region of the AGN, reducing the amount of observable X-ray radiation. Moreover, the torus obscures the optical broad emission lines produced in the broad-line region located within parsec scales from the nucleus, but it does not obscure the optical narrow emission lines produced at kpc scales from the nucleus. According to this picture, type 1 AGN show broad and narrow lines in their optical spectra as they are viewed face-on, while type 2 AGN only display narrow emission lines as they are viewed edge-on. This picture is confirmed by the presence of large amount of obscuration in the X-ray spectra of type 2 AGN and the little absorption in type 1 (e.g. Bassani et al. 1999; Risaliti, Maiolino & Salvati 1999).

The fraction of obscured AGN is important for the understanding of the nature of the circumnuclear medium, but it is also fundamental to characterize the history of black hole accretion in the Universe (Alexander et al. 2005; Gilli, Comastri & Hasinger 2007). Multi-wavelength surveys have attempted to constrain the number of obscured ($N_{\rm H} > 10^{22}$ cm^{-2}) and Compton thick (CT) AGN ($N_{\rm H} > 10^{24}$ cm^{-2}), in the optical (e.g. Risaliti et al. 1999; Cappi et al. 2006; Panessa et al. 2006; Akylas & Georgantopoulos 2009; Jia et al. 2013; Vignali et al. 2014), infrared (e.g. Fiore et al. 2009; Alexander et al. 2011; Brightman & Nandra 2011) and hard X-rays (e.g. Sazonov et al. 2008; Malizia et al. 2009; Burlon et al. 2011). Hard X-ray surveys should be able to detect obscured AGN with less biases; however, even at energies > 10 keV, part of the intrinsic flux is reduced by obscuration to a level below the survey detection limit of current missions, leading to an observed fraction of CT AGN of

★ E-mail: francesca.panessa@iaps.inaf.it

a few per cent (e.g. Ajello et al. 2008; Malizia et al. 2009, 2012; Burlon et al. 2011; Vasudevan, Mushotzky & Gandhi 2013); when correcting for biases, this fraction rises to around 20–30 per cent.

The fraction of obscured AGN appear to decrease with increasing observed X-ray luminosity in the local and distant Universe (e.g. Ueda et al. 2003, 2014; La Franca et al. 2005; Sazonov et al. 2007; Burlon et al. 2011; Aird et al. 2015a,b; Buchner et al. 2015). This effect is likely due to the decrease of the covering factor of the obscuring material with the luminosity; however, this result has been questioned by Sazonov, Churazov & Krivonos (2015). A similar dependence has been found also with redshift (the fraction of absorbed objects increases towards higher redshifts), although this result is more controversial (e.g. La Franca et al. 2005; Treister & Urry 2006; Ueda et al. 2014); even at $z > 2$, larger absorption fractions are found in high-luminosity AGN (Iwasawa et al. 2012).

In this work, we investigate the role of absorption in radio galaxies. Does the presence of a jet influence the level of obscuration in AGN? Radio galaxies launch relativistic jets on large scales (from sub-kpc to Mpc) and are strong emitters in the radio band. Fanaroff & Riley (1974) classified radio galaxies into two classes, based on their radio power and morphology: the low-luminosity radio galaxies (FR I) usually show a core, and twin jets (on average symmetric in brightness) which lose collimation at some distance from the core to form radio lobes; in the high-luminosity sources (FR II) the radio jets are faint, or invisible, and culminate in high surface brightness regions (hotspots), with the radio lobes being backflow emission. This morphological classification is not sharp, and intermediate and/or hybrid morphologies can be found (Capetti, Fanti & Parma 1995).

Radio galaxies have been also classified into low-excitation radio galaxies (LERGs) and high-excitation radio galaxies (HERGs) based on the optical emission lines from the nuclei (see Hine & Longair 1979). Most FR I and a subset of low radio power FR II are LERGs and also a few HERGs show an FR I morphology. It is believed that LERGs are inefficiently accreting objects and that their radio through X-ray nuclear emission is produced within their small-scale jet, while the emission in HERGs is likely accretion dominated (Chiaberge, Capetti & Celotti 2002; Hardcastle, Evans & Croston 2006). Moreover, HERGs show evidence for strong cosmic evolution at all radio luminosities, indicating a tendency of being located at larger distances, while LERGs are consistent with little or no evolution. A possible scenario is that HERGs might be fuelled at relatively high rates in radiatively efficient standard accretion discs by cold gas, perhaps brought in through mergers and interactions, and with some of the cold gas leading to associated star formation (Best & Heckman 2012). So far, no clear dividing factor between the FR I and FR II sources is found even when combining radio luminosity, accretion mode, large-scale environment and host galaxy luminosity (Gendre et al. 2013).

Early X-ray studies of radio galaxies revealed a large fraction of obscured nuclei, with narrow-line radio galaxies showing column densities between 10^{21} and 10^{24} cm^{-2}, in agreement with the unification predictions (Sambruna, Eracleous & Mushotzky 1999). An anti-correlation between the absorbing column density and the radio core dominance parameter is found, suggesting that the absorption increases as the jet orientation angle decreases, in agreement with the unified models (Grandi, Malaguti & Fiocchi 2006; Wilkes et al. 2013). Most of the X-ray studies on radio galaxies are based on individual sources, and only few works are performed on statistically significant samples. One example is the X-ray study of 22 radio galaxies which shows that FR I typically have much lower intrinsic absorption than FR II (Evans et al. 2006). Similarly, LERGs are generally X-ray weak with little or no absorption (Hardcastle et al. 2006), suggesting that the torus itself is missing or receding as a consequence of the inefficient accretion regime (Lawrence 1991). A large fraction of obscured AGN is also found in a larger sample of ∼40 narrow-line radio galaxies (Hardcastle, Evans & Croston 2009), but no CT radio galaxy is found. Recently, a study of 38 high-redshift ($1 < z < 2$) low-frequency-selected (178 MHz) 3CRR radio galaxies recovers a CT fraction of ∼20 per cent (Wilkes et al. 2013), found by means of multi-frequency diagnostics to unveil CT candidates otherwise missed by simple hardness ratio arguments. However, in the local Universe, only a handful of CT radio galaxies are found (e.g. Guainazzi et al. 2004, 2006; Hardcastle et al. 2006; Eguchi et al. 2009). This very low fraction of CT radio galaxies is puzzling and whether it is due to evolution or selection effect must be clarified.

Since 2002, *INTEGRAL*/Imager on Board the Integral Satellite (IBIS) and later on *Swift*/The Burst Alert Telescope (BAT) are surveying the sky at energies greater than 10 keV, releasing all sky catalogues that contain a large number of AGN, some previously known and others discovered for the first time at hard X-rays (Bird et al. 2010; Cusumano et al. 2010; Krivonos et al. 2010; Baumgartner et al. 2013). The hard X-ray selection is sensitive to gas rather than dust obscuration and should therefore allow the detection of highly obscured AGN, mostly mildly CT AGN with column densities in the range between 10^{24} and 10^{25} cm^{-2} where the continuum radiation should be visible above 10 keV.

In this work, we present for the first time the column density distribution of a sample of radio galaxies selected at hard X-rays from *INTEGRAL* and *Swift* observations. The paper is organized as follows: in Section 2 we present the radio galaxy sample and the X-ray data; in Section 3 we report on the column density distribution and comment on some peculiar objects; in Section 4 we discuss the fraction of obscured and CT AGN and in Section 5 we present our conclusions. Throughout this paper, we assume a flat Λ cold dark matter cosmology with $(\Omega_M, \Omega_\Lambda) = (0.3, 0.7)$ and a Hubble constant of 70 km s^{-1} Mpc^{-1} (Jarosik et al. 2011).

2 THE SAMPLE AND THE X-RAY DATA

For the purpose of this work, we have used the same sample of radio galaxies as in Bassani et al. (2016), except for three candidate sources for which the radio galaxy classification is uncertain and that we have not considered in this work. In Bassani et al. (2016), AGN from hard X-ray catalogues have been selected looking for extended radio emission. The hard X-ray catalogues considered are (1) the sample of 272 *INTEGRAL* AGN discussed by Malizia et al. (2012), with a few additional sources discovered or identified as AGN afterwards (Landi et al. 2010; Krivonos et al. 2012; Masetti et al. 2013), and (2) the 70-month *Swift*/BAT AGN catalogue of Baumgartner et al. (2013) which lists 822 objects associated with AGN or galaxies; a sample of 65 objects classified as 'unknown' has also been included in an attempt to uncover all possible radio galaxies in the BAT sample. In Bassani et al. (2016), the NRAO VLA Sky Survey (Condon et al. 1998) and the Sydney University Molonglo Sky Survey (Mauch et al. 2003) were used to assess the morphology and derive the radio power of the hard X-ray selected AGN. The morphological classification of our sample follows Fanaroff & Riley (1974), and is based on the radio morphology (core, jets, lobes and hotspots) and radio power, the transition power between FR I and FR II being roughly set at $\log P(1.4\ \mathrm{GHz}) = 24.5$ W Hz^{-1} (Owen & Laing 1989).

The final sample is made of 64 hard X-ray selected radio galaxies, 22 from Malizia et al. (2012) plus four additional *INTEGRAL* sources lately identified as radio galaxies:[1] 22 AGN are of type 1, 19 of type 2 and 21 of intermediate class. The intermediate AGN are themselves split into 12 objects of early-type (1.2–1.5) and 9 of late-type (1.8–1.9) Seyfert classification. One source in the sample, IGR J13107−5626, has no redshift or an optical classification, while PKS 1737−60 has a photometric redshift and no optical classification. The majority of the sample has a radio morphological classification as FR II, with only six FR I and six intermediate FR I/FR II. FR II are likely associated with HERGs (Buttiglione et al. 2009) accreting at high Eddington ratios; in this sense, their dominance is expected in a hard X-ray selected sample.

The X-ray fluxes and column densities are taken from the literature (see column 9 in Table 1 for references) except for 16 objects for which we have analysed X-Ray Telescope (XRT)+BAT broad-band spectra (see Appendix A for details on the X-ray analysis). In Fig. 1, we plot the 20–100 keV X-ray luminosity versus redshift (left-hand panel). It is clear that hard X-rays select nearby very luminous radio galaxies, with 20–100 keV luminosities ranging from 10^{42} to 10^{46} erg s^{-1}. Black hole masses have been collected from the literature (column 11 for references), ranging from $\sim 10^{7}$ to 10^{9} M$_{\odot}$.[2] In Fig. 1 (right-hand panel), we plot the distribution of the ratio between the bolometric luminosity and the Eddington luminosity (the bolometric luminosity is derived by applying a correction factor of 20 to the 2–10 keV luminosity; see Vasudevan & Fabian 2007). The Eddington ratios are relatively high suggesting that the hard X-ray radio galaxies are efficiently accreting sources and that their X-ray emission is likely dominated by the disc–corona system even in those galaxies with the most powerful jets (e.g. Reynolds et al. 2015). The only source accreting at a low Eddington rate is Cen A; for this source, it has been proposed that the hard X-ray emission is dominated by an advection-dominated accretion flow (e.g. Fuerst et al. 2016), and its detection is likely due to its closeness.

3 THE COLUMN DENSITY DISTRIBUTION

The column density distribution of radio galaxies has been studied in samples selected either in the X-rays (Sambruna et al. 1999) or in the radio (Evans et al. 2006; Hardcastle et al. 2009; Wilkes et al. 2013). Narrow-line radio galaxies typically show large X-ray column densities in agreement with the unified models; however, the number of CT AGN has always been very small, quite below the 20–50 per cent fraction observed in local non-radio galaxies samples. In the left-hand panel of Fig. 2, we report the column density distribution of type 1 (black histogram) and type 2 AGN (blue shaded histogram). Intermediate Seyfert galaxies of early-type classification (1.2–1.5) have been included in the type 1 group, while the late-type (1.8–1.9) intermediates are included in the type 2 group. As expected, type 2 radio galaxies are typically more absorbed than type 1, with the distribution peaking in the range between 10^{23} and 10^{24} cm^{-2}. In particular, sources with $N_{\rm H} > 10^{22}$ cm^{-2} are 26/64 ($\sim 40^{+13}_{-11}$ per cent) among the total sample and 21/28 (75^{+13}_{-9} per cent) among type 2 Seyferts are in agreement with the observed fractions found in optically selected samples of non-radio galaxies. On the other hand, only one source is CT (NGC 612) while VII Zw 292 has a column density consistent with the CT limit within an error of 90 per cent, implying that the observed fraction of CT AGN is around 2–3 per cent (<11 per cent) among the total sample and 4–7 per cent (< 23 per cent) among type 2 sources.[3]

When low-quality X-ray spectra do not allow a proper estimate of the real column density, it is possible to miss some CT AGN in a given sample. A diagram proposed by Malizia et al. (2007) uses the $N_{\rm H}$ versus softness ratio ($F_{2-10\,\rm keV}/F_{20-100\,\rm keV}$) to unveil hidden CT AGN; its validity has been proven by several other works (Ueda et al. 2007; Winter et al. 2008; Matt et al. 2012). Misclassified CT objects populate the part of the diagram with low absorption and low softness ratios, as the 2–10 keV flux is suppressed by absorption, while the 20–100 keV is less affected by absorption. The $N_{\rm H}$ versus the ratio between the observed 2–10 and 20–100 keV of the radio galaxy sample is plotted in Fig. 2 (right-hand panel): no source populates the bottom-left part of the diagram suggesting that there are no hidden mildly CT AGN in the sample.

3.1 X-ray absorption versus optical and radio classification

Similarly to what found in non-radio galaxies' hard X-ray samples, a small fraction of objects are 'outliers', i.e. exceptions to the unified models such as type 1 AGN with absorption and type 2 AGN without absorption (see Malizia et al. 2012). Six objects with broad emission lines (type 1, type 1.2 and type 1.5) display column densities > 10^{22} cm^{-2}. IGR J17488−2338 and 4C 50.55 are absorbed by one (Malizia et al. 2014) and two (Molina et al. 2007) layers of cold material partially covering the central source, respectively. Similarly in 3C 227 and PKS 2135−14, intrinsic absorption has been measured from the *Chandra* spectrum (Mingo et al. 2014). The *XMM–Newton* spectrum of IGR J14488−4008 is characterized by absorption due to ionized elements (Molina et al. 2015), and the presence of a warm absorber component is also found in 3C 445 (Torresi et al. 2012). It is therefore likely that in most of these type 1 AGN ionized material located just off the torus and/or accretion disc might be responsible for the X-ray absorption.

Type 2 objects without X-ray absorption are another type of 'outliers' with respect to the unified models, where a column density <10^{21} cm^{-2} is not enough to obscure the broad-line region, and the lack of broad emission lines in the optical spectrum is likely due to an absent or very weak broad-line region (Panessa & Bassani 2002; Bianchi et al. 2012). In this sample, only PKS 2331−240 is a type 2 radio galaxy without absorption, and it is the subject of a recent multi-wavelength observational campaign conducted by our team, which will be presented in a forthcoming publication.

Osterbrock (1981) introduced the notations Seyfert 1.5, 1.8 and 1.9, where the subclasses are based on the optical appearance of the spectrum, with the numerically larger subclasses having weaker broad-line components relative to the narrow-line ones. According to unified models, these intermediate classifications should correspond to an intermediate inclination of the line of sight with respect

[1] IGR J13107−5626 from Bassani et al. (2016), IGR J14488−4008 from Molina et al. (2015), IGR J17488−2338 from Molina et al. (2014) and 4C+21.55 from Bassani et al. (2016), and 60 from the *Swift*/BAT AGN catalogue. 22 sources have been detected both by *INTEGRAL* and *Swift*/BAT. Radio galaxies represent ∼7–10 per cent of the total AGN population at hard X-rays.The sample is presented in Table 1. In column 3, we report the optical classification of the sample (see Bassani et al. 2016).

[2] Different methods have been used in the literature to estimate the black hole mass; therefore, the values reported are not homogeneously derived, introducing a source of uncertainty which is difficult to estimate.

[3] Throughout the paper, the standard error on the sample proportions in the binomial standard deviation for small samples is calculated at 2σ (Gehrels 1986).

Table 1. Radio galaxies detected by *INTEGRAL*/IBIS and *Swift*/BAT.

Name	z	Opt class	Radio morphology	log N_H	F(2–10 keV)†	F_{BAT}† (20–100 keV)	F_{IBIS}† (20–100 keV)	Ref.	log M_{BH}	Ref.	R_{core}	Ref.
PKS 0018−19	0.095 579	Sy1.9	FR II	21.89 [21.83 – 21.95]	1.07	1.19	–	1	–	–	0.186	1
PKS 0101−649	0.163 000	BLQSO	FR II	**20.36**	0.31	0.63	–	1	–	–	–	–
3C 033	0.059 700	Sy2	FR II	23.72 [23.69 – 23.80]	0.27	1.71	–	2	8.48	1	0.003	2
NGC 612	0.029 771	Sy2	FR I/II	24.04 [24.02 – 24.06]	1.60	3.04	–	3	8.64	1	0.009	3
3C 059	0.109 720	Sy1.8	FR II	**20.78**	0.84	1.07	–	4	7.15	2	0.034	4
3C 062	0.147 000	Sy2	FR II	23.26 [23.18 – 23.36]	0.2	0.77	–	5	8.81	1	0.005	1
4C +10.08	0.070 000	NLRG	FR II	21.89[21.69 – 22.05]	0.23	0.87	–	1	–	–	–	–
QSO B0309+411B	0.134 000	Sy1	FR II	**21.11**	2.36	0.96	1.90	6	–	–	3.0	5
2MASX J03181899+6829322	0.090 100	Sy1.9	FR II	22.61 [22.57 – 22.66]	0.73	1.03	1.34	6	–	–	0.133	6
NGC 1275	0.017 559	Sy1.5	FR I	21.08 [21.04 – 21.11]	1.23	3.80	3.00	6	8.5	3	0.646	7
3C 098	0.0304	Sy2	FR II	23.08 [23.00 – 23.18]	0.27	–	3.80	6	7.88	4	0.0017 ± 0.0005	8
3C 105	0.089 000	Sy2	FR II	23.45 [23.40 – 23.47]	0.21	1.69	3.10	6	8.61	5	0.006	3
3C 109	0.305 600	Sy1.8	FR II	21.70 [21.60 – 21.78]	0.80	0.82	–	7	8.30	6	0.06 ± 0.02	8
3C 111	0.048 500	Sy1	FR II	21.66 [21.63 – 21.69]	3.51	7.13	10.50	6	8.80	7	0.04 ± 0.02	8
3C 120	0.033 010	Sy1	FR I?	21.10 [21.19 – 21.22]	4.60	5.73	7.58	6	7.75	7	0.67	3
PKS 0442−28	0.147 000	Sy2	FR II	21.93 [21.73 – 22.07]	1.16	1.14	–	5	9.11	5	0.041	9
Pic A	0.035 058	Liner/Sy1	FR II	**20.78**	1.13	2.36	3.24	6	8.70	7	0.07	3
PKS 0521−364	0.056 546	Sy1	FR I/II	**20.55**	1.10	2.00	2.19	6	8.6	8	0.176	3
PKS 0707−35	0.110 800	Sy2	FR II	22.71[22.38 – 22.72]	0.56	1.19	–	8	–	–	–	–
3C 184.1	0.118 200	Sy2	FR II	23.03[22.88 – 23.16]	0.26	0.69	–	9	8.32	9	–	–
B3 0749+460A	0.051 799	Sy1.9	FR II	**20.25**	0.30	0.84	–	1	6.9	10	–	–
3C 206	0.197 870	Sy1.2	FR II	**20.75**	1.50	1.52	–	8	8.86	11	0.273	1
4C +29.30	0.064 715	Sy2	FR I/II	23.70 [23.68 – 23.71]	0.11	0.95	–	10	8.2	12	0.429 ± 0.134	8
3C 227	0.086 272	Sy1.5	FR II	22.16 [22.10 – 22.22]	2.36	1.52	–	5	8.90	7	0.0123	3
VII Zw 292	0.058 100	Sy2	FR II	23.96 [23.80 – 24.16]	0.08	0.94	–	11	–	–	0.006	10
3C 234	0.184 925	Sy1.9	FR II	23.81 [23.79 – 23.83]	0.13	0.48	–	12	8.99	13	0.02 ± 0.006	8
PKS 1143−696	0.244 000	Sey1.2	FR II	**21.21**	0.54	0.92	1.28	6	8.62	14	–	–
IGR J13107−5626	–	–	FR II?	23.59 [23.41 – 23.80]	0.11	1.02	0.87	13	–	–	–	–
Cen A	0.000 88	Sey2	FR I	23.17 [23.16 – 23.18]	21.20	82.73	59.00	6	9.11	15	0.125	3
Cen B	0.012 916	NLRG	FR I/II	21.11 [21.98 – 22.21]	0.49	–	1.77	6	–	–	0.07 ± 0.02	8
3C 287.1	0.2156	Sy 1	FR II	**21.21**	0.28	–	1.50	6	8.49	16	0.365 ± 0.114	8
2MASX J14364961−1613410	0.144 537	BLQSO	FR I/II	**20.88**	0.72	1.08	–	1	8.64	17	–	–
IGR 14488−4008	0.123	Sey1.2	FR II	22.89 [22.74 – 23.04]	0.53	0.82	0.60	14	8.58	14	–	–
3C 309.1	0.905 000	Sy1.5	C	<20.50	0.17	0.54	–	15	9.1	18	1.87 ± 0.58	8
4C +63.22	0.204 00	Sy1	FR II	**20.17**	0.36	0.56	–	1	–	–	0.028	10
3C 323.1	0.264 300	Sy1.2	FR II	20.78 [20.00 – 21.04]	0.55	0.64	–	16	9.12	19	0.046 ± 0.014	8
4C +23.42	0.118 000	Sy1	FR I	21.75 [21.60 – 21.86]	0.32	0.79	–	1	–	–	–	–
Leda 100168	0.183 000	Sy1	FR II	<20.69	0.43	0.74	–	1	–	–	–	–
3C 332	0.151 019	Sy1	FR II	**20.30**	0.58	1.34	–	4	8.64	16	–	–
Mrk 1498	0.054 700	Sy1.9	FR II	23.76 [23.67 – 23.84]	0.90	2.69	–	17	8.59	20	0.09	11
4C +34.47	0.206 000	Sy1	FR II	**20.49**	0.94	1.24	–	18	8.01	11	0.86 ± 0.26	8
PKS 1737−60	0.410 000 Phot	–	FR II	**20.77**	0.73	0.84	–	1	–	–	–	–
4C +18.51	0.186 000	Sy1	FR II	**20.74**	0.49	0.59	–	1	9.35	21	0.1	12
IGR J17488−2338	0.240	Sy1.5	FR II	22.06 [21.96 – 22.15]	0.20	–	1.40	19	9.11	14	0.179	13

Table 1 – *continued*

Name	z	Opt class	Radio morphology	log $N_{\rm H}$	F(2–10 keV)†	$F_{\rm BAT}$† (20–100 keV)	$F_{\rm IBIS}$† (20–100 keV)	Ref.	log $M_{\rm BH}$	Ref.	$R_{\rm core}$	Ref.
3C 380	0.692 000	Sy1.5	FR II	**20.75**	0.40	0.96	–	20	9.4	18	0.817 ± 0.254	8
3C 382	0.057 870	Sy1	FR II	**20.79**	5.98	5.32	4.24	6	8.90	21	0.05 ± 0.02	8
3C 390.3	0.056 100	Sy1.5	FR II	**20.63**	2.14	6.20	5.90	6	8.80	21	0.09 ± 0.03	8
PKS 1916−300	0.166 819	Sy1.5/1.8	FR II	**20.90**	0.62	0.97	0.99	6	–	–	0.02	14
3C 403	0.059 000	Sy2	FR II	23.65 [23.58 – 23.62]	1.30	1.96	1.87	6	8.96	5	0.004	3
Cygnus A	0.056 075	Sy1.9	FR II	23.30 [23.25 – 23.32]	1.20	8.29	8.49	6	9.40	22	0.002	3
PKS 2014−55	0.060 629	Sy2	FR I	23.51 [23.36 – 23.64]	0.39	1.94	–	1	–	–	–	–
4C +21.55	0.173 500	Sy1	FR II	21.78 [21.62 – 22.09]	1.40	1.98	2.91	21	–	–	–	–
4C +74.26	0.104 000	Sy1	FR II	21.15 [21.04 – 21.20]	2.53	3.18	4.16	6	9.37	7	0.95 ± 0.29	8
S5 2116+81	0.084 000	Sy1	FR I	**21.38**	1.21	2.14	3.04	6	8.12	7	1.80 ± 0.54	8
4C 50.55	0.020 000	Sy1	FR II	22.89 [22.79 – 22.99]	4.88	12.25	12.50	6	7.80	23	0.1	15
3C 433	0.101 600	Sy2	FR I/FR II	22.94 [22.90 – 23.97]	0.10	1.02	–	22	9.10	24	0.0011 ± 0.0003	8
PKS 2135−14	0.200 47	Sy1.5	FR II	23.26 [23.02 – 23.48]	0.57	0.90	–	5	9.65	5	0.096	3
PKS 2153−69	0.028 273	Sy1	FR II	**20.40**	0.72	0.84	–	9	–	–	0.03 ± 0.01	8
2MASX J22194971+2613277	0.085 000	Sy1	FR II	21.40 [21.30 – 21.49]	0.67	1.03	–	1	–	–	–	–
3C 445	0.055 879	Sy1.5	FR II	23.35 [23.26 – 23.46]	0.67	2.63	–	23	8.89	5	0.04	3
3C 452	0.081 100	Sy2	FR II	23.77 [23.70 – 23.83]	0.50	1.97	2.75	6	8.54	13	0.06 ± 0.018	8
PKS 2300−18	0.128 929	Sy1	FR II?	**20.34**	0.51	0.70	–	1	8.25	25	1.07	1
PKS 2331−240	0.047 700	Sy2	FR II	**20.21**	0.71	0.85	–	1	–	–	0.65	16
PKS 2356−61	0.096 306	Sy2	FR II	23.17 [23.13 – 23.21]	0.20	0.91	–	5	8.96	5	0.008	3

Note. Bold face value of column 5 are upper limits to the X-ray column density.

†The 2–10 and 20–100 keV fluxes are in units of 10^{-11} erg cm^{-2} s^{-1}. X-ray references: 1. This work, 2. Torresi et al. (2009), 3. Eguchi et al. (2011), 4. Tombesi et al. (2014), 5. Mingo et al. (2014), 6. Malizia et al. (2012), 7. Hardcastle et al. (2006), 8. Tazaki et al. (2013), 9. Grandi et al. (2006), 10. Sobolewska et al. (2012), 11. Evans et al. (2008), 12. Vasudevan et al. (2013), 13. Landi et al. (2010), 14. Molina et al. (2015), 15. Siemiginowska et al. (2008), 16. Hasenkopf, Sambruna & Eracleous (2002), 17. Eguchi et al. (2009), 18. Page et al. (2004), 19. Molina et al. (2014), 20. Belsole, Worrall & Hardcastle (2006), 21. Malizia et al. (2016), 22. Miller & Brandt (2009), 23. Sambruna, Reeves & Braito (2007). Black hole mass references: 1. Bettoni et al. (2003), 2. Wandel (2002), 3. Wilman, Edge & Johnstone (2005), 4. Woo & Urry (2002), 5. Mingo et al. (2014), 6. McLure et al. (2006), 7. Kataoka et al. (2011), 8. Sbarrato et al. (2012), 9. Grandi et al. (2006), 10. Greene & Ho (2007), 11. Liu, Jiang & Gu (2006), 12. Sobolewska et al. (2012), 13. Marchesini, Celotti & Ferrarese (2004), 14. Masetti et al. (2013), 15. Sadoun & Colin (2012), 16. Mezcua et al. (2011), 17. Kim et al. (2008), 18. Wu (2009), 19. Runnoe et al. (2013), 20. Winter et al. (2010), 21. Wang, Mao & Wei (2009), 22. Tadhunter et al. (2003), 23. Tazaki et al. (2010), 24. Cao & Rawlings (2004), 25. Wu & Liu (2004). 5 GHz radio core dominance references: 1. Reid, Kronberg & Perley (1999), 2. Hardcastle, Birkinshaw & Worrall (1998), 3. Morganti, Killeen & Tadhunter (1993), 4. Bondi et al. (1993), 5. de Bruyn et al. (1989), 6. Schoenmakers et al. (1998), 7. Abdo et al. (2010), 8. Fan & Zhang (2003), 9. Morganti et al. (1999), 10. Lara et al. (2001), at 1.4 GHz; 11. Rottgering et al. (1996), 12. Lister, Gower & Hutchings (1994), 13. Molina et al. (2014), 14. Duncan & Sproats (1992), 15. Molina et al. (2007), 16. Slee et al. (1994).

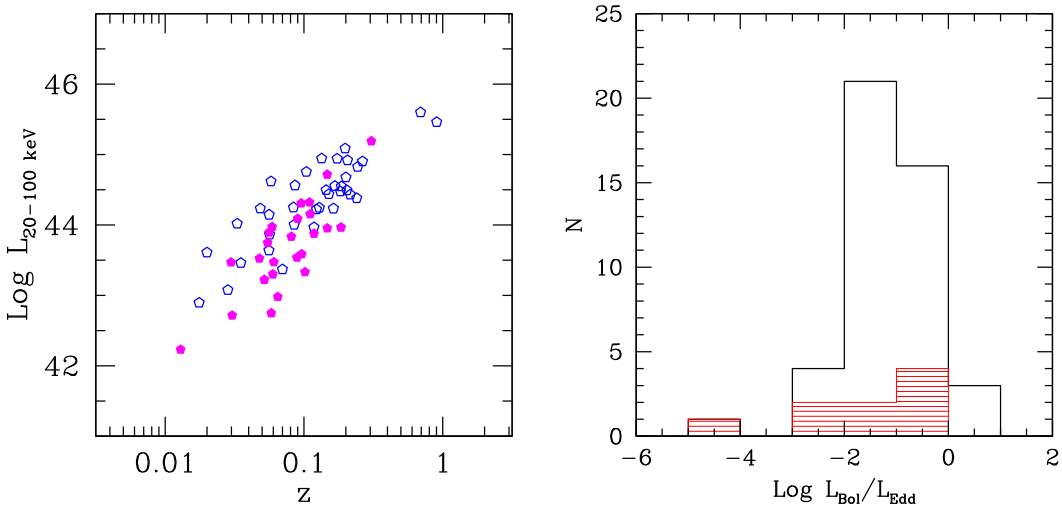

Figure 1. Bilogarithmic plot of the 20–100 keV luminosity versus redshift (left-hand panel), blue open points are type 1 AGN, while magenta filled points are type 2 AGN. The right-hand panel shows the distribution of the ratio between the bolometric luminosity and the Eddington luminosity for the total sample, where red shaded histogram represents FR I and intermediate FR I/FR II radio galaxies.

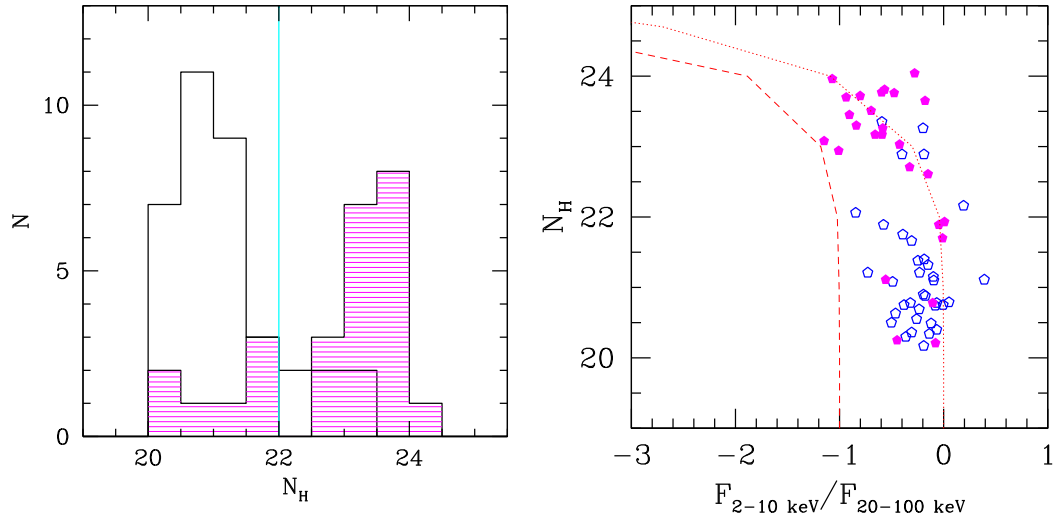

Figure 2. Column density distribution in cm^{-2}; type 1 are represented by the black histogram while type 2 by the magenta shaded histogram (left-hand panel). A cyan line separates obscured objects ($N_H > 10^{22}$ cm^{-2}) from unobscured objects. Column density distribution in cm^{-2} versus the $F_{2-10\,keV}/F_{20-100\,keV}$ (right-hand panel). Blue open points are type 1 AGN, while magenta filled points are type 2 AGN. Lines correspond to expected values for an absorbed power law with photon indices 1.5 (dotted) and 1.9 (dashed) as in Malizia et al. (2012).

to the obscuring torus; therefore, type 1.8–1.9 should be mildly absorbed at X-rays (Risaliti et al. 1999). In our sample, three sources are classified as type 1.8 Seyferts (3C 059, B3 0749+460A and PKS 1916−300) and show absorption consistent with the Galactic one, suggesting that the broad-line components maybe intrinsically weak. However, Trippe et al. (2010) have shown that a large fraction of 1.8 and 1.9 were misclassified due to an overestimation of the flux of broad Hα, while others received this designation because of their low continuum flux. Accurate observations at multiple epochs are therefore necessary to explore these possibilities.

In previous surveys, FR I radio galaxies have usually shown less absorption than FR II. In this sample, FR I and intermediate FR I/FR II, though numerically inferior, display a column density distribution similar to that of FR II. Interestingly, two out of five of the FR I in the sample are heavily absorbed (Cen A and PKS 2014−55). Three out of six intermediate FR I/FR II show $N_H > 5 \times 10^{22}$ cm^{-2}, i.e. 4C+29.30, 3C 433 and NGC 612.

3.2 The radio core dominance versus absorption

The radio core dominance is defined as $R_{core} = S_{core}/(S_{tot} - S_{core})$, where S_{core} and S_{tot} are the core and the total flux densities at 5 GHz, respectively. It has been used as an orientation indicator, as objects with a large R_{core} should emit their radiation in a direction closer to the line of sight. Indeed, a strong anti-correlation between the X-ray column density and R_{core} has been found in samples of radio galaxies (e.g. Grandi et al. 2006; Wilkes et al. 2013). A significant anti-correlation between R_{core} and the inclination of the dusty torus (derived from modelling the infrared spectral energy distribution) has also been found (Drouart et al. 2012). We have collected

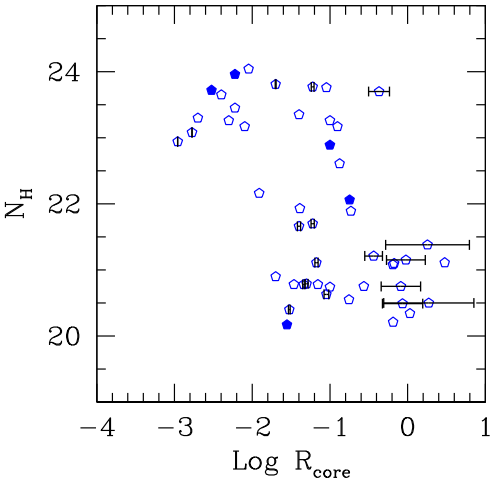

Figure 3. Column density versus the radio core dominance parameter R_{core} estimated at 5 GHz. Filled points have an R_{core} estimated at 1.4 GHz.

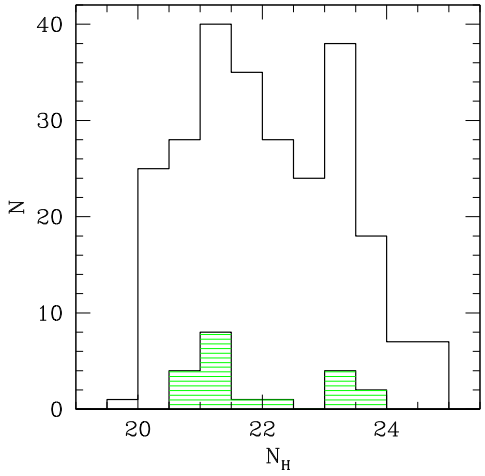

Figure 4. Column density distribution of non-radio galaxies (black histogram) and radio galaxies (shaded green) of Malizia et al. (2012).

the R_{core} values at 5 GHz.[4] We have correlated the X-ray column density with R_{core} (see Fig. 3). The Spearman's rho correlation coefficient is −0.50 with a two-tailed value of the null hypothesis probability of correlation of 0.000 27, suggesting that also among our sample of radio galaxies the two quantities are anti-correlated, in agreement with unified models. No correlation is found between R_{core} and the 2–10 keV luminosity or the 20–100 keV luminosity. Note, however, that the calculation of R_{core} parameter relies on data taken at different epochs, with different instruments and at different linear scales. An appropriate set of radio images at the same frequency and with about the same linear resolution is fundamental in this respect for a proper determination of the radio core dominance parameter.

4 THE FRACTION OF ABSORBED AND CT RADIO GALAXIES

The determination of an intrinsic column density distribution, not affected by biases, is a hard task, even for the current hard X-ray surveys, where above 10–15 keV a significant fraction (up to 50–60 per cent) is missed for $N_H > 3 \times 10^{24}$ cm^{-2} (Ajello et al. 2009; Malizia et al. 2009). Therefore, the absorption bias limits the detection of CT objects only to those with bright fluxes and in the very local Universe. Malizia et al. (2009) recover a fraction of 20–30 per cent of CT by limiting the sample to $z<0.015$; similarly Burlon et al. (2011) have found a fraction of 20 per cent CT AGN by correcting for the absorption bias in the *Swift*/BAT sample. In order to evaluate the distance and flux biases among hard X-ray selected radio galaxies, we have estimated the fraction of absorbed and CT AGN in a sample containing both non-radio galaxies and radio galaxies selected at hard X-rays and therefore, subject to the same bias effects. We have considered the total *INTEGRAL* AGN sample in Malizia et al. (2012) in which 22 out of 271 AGN are radio galaxies. In Fig. 4, we present the column density distribution of non-radio galaxies (black histogram) and radio galaxies (green shaded histogram). The fraction of absorbed AGN is 49^{+6}_{-7} per cent (121/249) among non-radio galaxies compared to 36^{+21}_{-16} per cent (8/22) among radio galaxies, while the fraction of CT AGN is 6±3 per cent (14/249) compared to 0/22 (<1. 3 per cent) among radio galaxies.

In Fig. 5 (right-hand panel), we have compared the redshift distribution of non-radio galaxies and radio galaxies (in green) separately. We have tested the null hypothesis that the two samples are taken from populations with the same redshift distribution using the Kolmogorov–Smirnov (KS) test at a significance level of $\alpha = 0.01$. The derived p-value is 0.0014; therefore, the null hypothesis can be rejected at the 1 per cent level. It is remarkable that no radio galaxies are found below $z<0.01$ (except for the peculiar source Cen A) in agreement with the fact that HERGs are preferentially found at larger distances than LERGs.

Excluding Cen A, we have selected all non-radio galaxies in Malizia et al. (2012) in the redshift regime where all radio galaxies are found, i.e. $z>0.01$. We have then compared the column density distribution of the two selected sub-samples. At these redshifts, the observed fraction of absorbed AGN among non-radio galaxies is 42^{+7}_{-6} per cent (89/212) consistent with the observed fraction in radio galaxies of 33^{+22}_{-16} per cent (7/21); similarly the fraction of CT sources among non-radio galaxies is 9/212 (4^{+4}_{-2} per cent) compared with that of radio galaxies (0/21, <1. 4 per cent). In Fig. 5 (left-hand panel), the 2–10 keV flux distribution of non-radio galaxies and radio galaxies (in green) is shown. In this case, the derived KS p-value is 0.047; therefore, the null hypothesis that the two samples are taken from populations with the same flux distribution cannot be rejected at the 1 per cent level. No radio galaxies are found below $\sim 10^{-12}$ erg cm^{-2} s^{-1}; therefore, we have selected all non-radio galaxies with $F_{2-10\,keV} > 10^{-12}$ erg cm^{-2} s^{-1}. In this case, the fraction of CT objects among non-radio galaxies (14/227, 6^{+4}_{-2} per cent) is only slightly larger than that of radio galaxies, 0/22 (<1. 3 per cent), while the fraction of absorbed AGN in non-radio galaxies (107/227, 47^{+7}_{-6} per cent) is again consistent within errors with that of radio galaxies (8/22, 36^{+21}_{-16} per cent). The above results suggest that radio galaxies might be affected by the same redshift bias as non-radio galaxies, suggesting that we are probably missing CT AGN in both classes of objects. However, the marginal evidence of a lower fraction of CT AGN in radio galaxies deserves deeper investigation through larger samples of objects.

[4] For five objects data were available at 1.4 GHz, while R_{core} in Fan & Zhang (2003) were calculated using extended luminosities at 1.4 GHz, assuming two possible values of the spectral index ($\alpha = 0.5$ and 1.0) to convert the 1.4 GHz luminosity into 5 GHz luminosity (see their work for details).

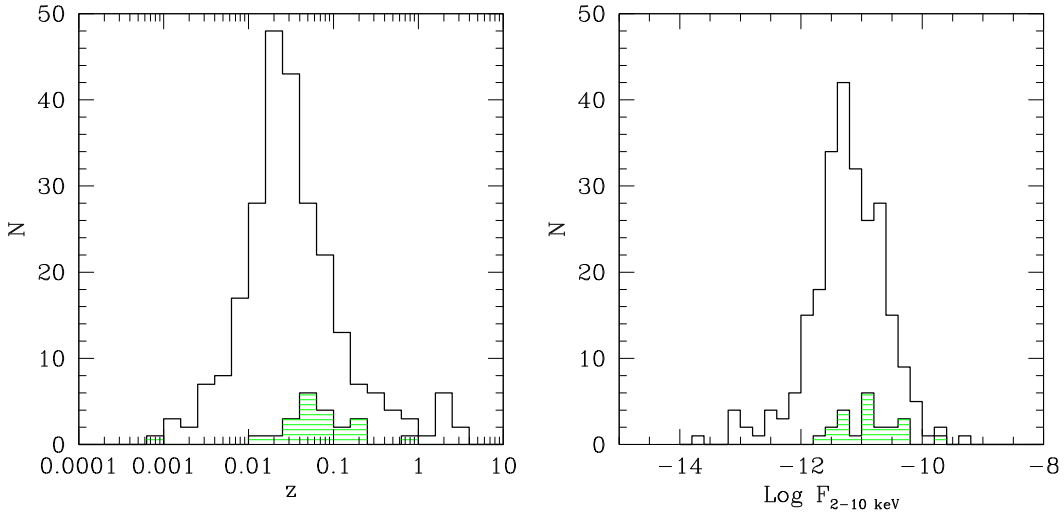

Figure 5. Left-hand panel: redshift distribution of non-radio galaxies and radio galaxies (shaded green) of the Malizia et al. (2012) *INTEGRAL* sample. Right-hand panel: 2–10 keV flux distribution of non-radio galaxies and radio galaxies (shaded green) of the Malizia et al. (2012) *INTEGRAL* sample.

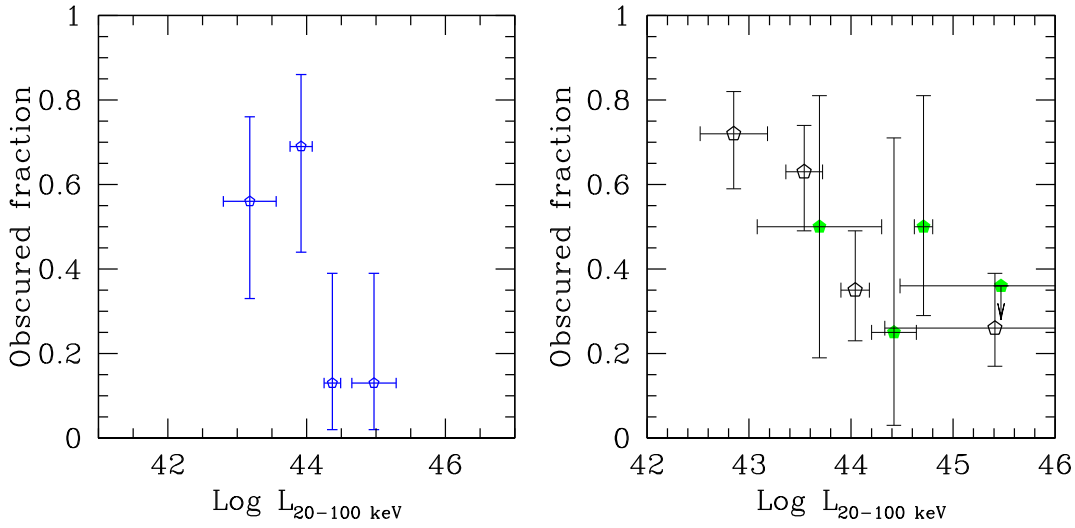

Figure 6. Fraction of obscured AGN (number of objects with $N_H > 10^{22}$ cm^{-2} over the total number) versus luminosity bins, computed for the 64 hard X-ray selected radio galaxies (left-hand panel). Fraction of obscured AGN versus luminosity bins, computed for the Malizia et al. (2012) sample (right-hand panel). Non-radio galaxies are drawn as black open polygons, while radio galaxies as green filled polygons.

We have explored a possible dependence of the observed fraction of absorbed AGN with luminosity. In Fig. 6, we show the dependence of the absorbed fraction in our sample of 64 radio galaxies with the intrinsic hard X-ray luminosity (left-hand panel). Sources have been grouped in order to have nearly the same number of objects in each bin. We find a trend of decreasing obscured sources with luminosity, in agreement with the results from X-ray surveys. We have done the same exercise on the sample by Malizia et al. (2012), separating radio galaxies from non-radio galaxies (right-hand panel). Unfortunately, the number of radio galaxies is very small, generating very large error bars; none the less, the fraction of obscured radio galaxies seems to follow the same trend in luminosity as obscured non-radio galaxies. A dependence of obscured sources with redshift cannot be tested with our flux-limited sample, as it would suffer from observational biases. However, a possible evolution of the CT radio galaxies population with redshift was suggested by the work from Wilkes et al. (2013), who have estimated a fraction of CT AGN of 21 ± 0.7 per cent in high-redshift radio galaxies ($1 < z < 2$). A confirmation to this result must come from the study of large samples at different redshift ranges.

5 CONCLUSIONS

We have presented for the first time the observed column density distribution of a sample of hard X-ray selected radio galaxies. The sample consists of 64 radio galaxies (mostly FR II), all within $z<1$, of relatively high luminosities (from 10^{42} to 10^{46} erg s^{-1}) and accreting at high Eddington ratios. All of them have an accurate measure of the column density and an accurate optical classification (except for two sources). Similarly to non-radio hard X-ray selected sources, we have found a fraction of ∼40 per cent of absorbed sources among the total sample, and ∼75 per cent among type 2 AGN. On the other hand, the observed fraction of CT AGN is ∼2–3 per cent compared to the 5–7 per cent found in non-radio galaxies' hard X-ray selected AGN (Malizia et al. 2009; Burlon et al. 2011).

These results confirms that, at the zeroth order, unified models apply in a similar way to AGN with jets. This is also confirmed by a recent study from Gupta, Sikora & Nalewajko (2016) in which the dust covering factors of FR II and quasars show a very similar distribution, suggesting similar accretion conditions on parsec scales among the two classes.

Among radio galaxies, a handful of objects apparently deviate from the unified model predictions, i.e. the optical classification does not match with the X-ray classification. Six objects display broad emission lines in their optical spectra but their X-ray spectra are absorbed. However, the absorption usually comes from ionized material not associated with the classical torus; therefore, the unified model predictions are not invalidated. One object is a type 2 AGN and has no X-ray absorption. Our simultaneous multi-frequency observations will allow us to rule out variability as a possible cause for such mismatch.

Finally, we have estimated the absorption and CT fractions in a sample of non-radio galaxies and radio galaxies extracted from the same sample selected at hard X-ray (from Malizia et al. 2012) and therefore subject to the same bias effects. We find that the fraction of absorbed AGN is comparable among non-radio galaxies and radio galaxies (49^{+6}_{-7} and 35^{+22}_{-17} per cent, respectively) while the fraction of CT AGN is only slightly larger in non-radio galaxies (6 ± 3 per cent) compared to radio galaxies (<1.4 per cent). We have selected one non-radio galaxy and one radio galaxy sub-sample in the same redshift range and then in the same flux range in order to exclude further biases, and overall we find that the fraction of absorbed AGN is always comparable (within errors) among the two groups, while there is marginal evidence that the fraction of CT is always slightly smaller in radio galaxies. We have also checked for a possible dependence of the absorbed population on the luminosity as suggested in the literature. We found that the fraction of absorbed radio galaxies decreases with luminosity as well as non-radio galaxies. Unfortunately, the small number of sources tested here prevent us from drawing a firm conclusion. Ideally, statistically significant samples at different redshifts are needed to confirm such a trend. *INTEGRAL* and *Swift* are continuing in their survey of the hard X-ray sky reaching sensitivity levels down to 10^{-12} erg cm^{-2} s^{-1} allowing us to detect new sources and to increase the sample of non-radio galaxies and radio galaxies (Bird et al. 2016; Malizia et al. 2016; Mereminskiy et al. 2016). In the future, *Square Kilometre Array* surveys will trace the low-power radio-loud AGN population at a flux level of 1 μJy (Prandoni & Seymour 2015) and in synergy with *Athena* it will be possible to investigate the evolution of the fraction of absorbed objects with X-ray luminosity and redshift up to $z \sim 4$–5.

ACKNOWLEDGEMENTS

FP acknowledges support from *INTEGRAL* ASI/INAF no. 2013-025-R.0. FP thanks Matteo Guainazzi and Paola Grandi for helpful discussions. The authors acknowledge the use of NED, SIMBAD and HEASARC.

REFERENCES

Abdo A. A. et al., 2010, ApJ, 720, 912
Aird J., Coil A. L., Georgakakis A., Nandra K., Barro G., Pérez-González P. G., 2015a, MNRAS, 451, 1892
Aird J. et al., 2015b, ApJ, 815, 66
Ajello M. et al., 2008, ApJ, 673, 96
Ajello M. et al., 2009, ApJ, 699, 603
Akylas A., Georgantopoulos I., 2009, A&A, 500, 999
Alexander D. M., Bauer F. E., Chapman S. C., Smail I., Blain A. W., Brandt W. N., Ivison R. J., 2005, ApJ, 632, 736
Alexander D. M. et al., 2011, ApJ, 738, 44
Antonucci R., 1993, ARA&A, 31, 473
Bassani L., Dadina M., Maiolino R., Salvati M., Risaliti G., Della Ceca R., Matt G., Zamorani G., 1999, ApJS, 121, 473
Bassani L., Venturi T., Molina M., Malizia A., Dallacasa D., Panessa F., Bazzano A., Ubertini P., 2016, MNRAS, in press
Baumgartner W. H., Tueller J., Markwardt C. B., Skinner G. K., Barthelmy S., Mushotzky R. F., Evans P. A., Gehrels N., 2013, ApJS, 207, 19
Belsole E., Worrall D. M., Hardcastle M. J., 2006, MNRAS, 366, 339
Best P. N., Heckman T. M., 2012, MNRAS, 421, 1569
Bettoni D., Falomo R., Fasano G., Govoni F., 2003, A&A, 399, 869
Bianchi S. et al., 2012, MNRAS, 426, 3225
Bird A. J. et al., 2010, ApJS, 186, 1
Bird A. J. et al., 2016, ApJS, 223, 15
Bondi M., Gregorini L., Padrielli L., Parma P., 1993, A&AS, 101, 431
Brightman M., Nandra K., 2011, MNRAS, 414, 3084
Buchner J. et al., 2015, ApJ, 802, 89
Burlon D., Ajello M., Greiner J., Comastri A., Merloni A., Gehrels N., 2011, ApJ, 728, 58
Buttiglione S., Capetti A., Celotti A., Axon D. J., Chiaberge M., Macchetto F. D., Sparks W. B., 2009, A&A, 495, 1033
Cao X., Rawlings S., 2004, MNRAS, 349, 1419
Capetti A., Fanti R., Parma P., 1995, A&A, 300, 643
Cappi M. et al., 2006, A&A, 446, 459
Chiaberge M., Capetti A., Celotti A., 2002, A&A, 394, 791
Condon J. J., Cotton W. D., Greisen E. W., Yin Q. F., Perley R. A., Taylor G. B., Broderick J. J., 1998, AJ, 115, 1693
Cusumano G., La Parola V., Romano P., Segreto A., Vercellone S., Chincarini G., 2010, MNRAS, 406, L16
de Bruyn A. G., 1989, A&A, 226, L13
Drouart G. et al., 2012, A&A, 548, A45
Duncan R. A., Sproats L. N., 1992, Proc. Astron. Soc. Aust., 10, 16
Eguchi S., Ueda Y., Terashima Y., Mushotzky R., Tueller J., 2009, ApJ, 696, 1657
Eguchi S., Ueda Y., Awaki H., Aird J., Terashima Y., Mushotzky R., 2011, ApJ, 729, 31
Evans D. A., Worrall D. M., Hardcastle M. J., Kraft R. P., Birkinshaw M., 2006, ApJ, 642, 96
Evans D. A., Hardcastle M. J., Lee J. C., Kraft R. P., Worrall D. M., Birkinshaw M., Croston J. H., 2008, ApJ, 688, 844
Fan J. H., Zhang J. S., 2003, A&A, 407, 899
Fanaroff B. L., Riley J. M., 1974, MNRAS, 167, 31p
Fiore F. et al., 2009, ApJ, 693, 447
Fuerst F. et al., 2016, ApJ, 819, 150
Gehrels N., 1986, ApJ, 303, 336
Gendre M. A., Best P. N., Wall J. V., Ker L. M., 2013, MNRAS, 430, 3086
Gilli R., Comastri A., Hasinger G., 2007, A&A, 463, 79
Grandi P., Malaguti G., Fiocchi M., 2006, ApJ, 642, 113
Greene J. E., Ho L. C., 2007, ApJ, 670, 92
Guainazzi M., Siemiginowska A., Rodriguez-Pascual P., Stanghellini C., 2004, A&A, 421, 461
Guainazzi M., Siemiginowska A., Stanghellini C., Grandi P., Piconcelli E., Azubike Ugwoke C., 2006, A&A, 446, 87
Gupta M., Sikora M., Nalewajko K., 2016, preprint (arXiv:1603.03670)
Hardcastle M. J., Birkinshaw M., Worrall D. M., 1998, MNRAS, 294, 615
Hardcastle M. J., Evans D. A., Croston J. H., 2006, MNRAS, 370, 1893
Hardcastle M. J., Evans D. A., Croston J. H., 2009, MNRAS, 396, 1929
Hasenkopf C. A., Sambruna R. M., Eracleous M., 2002, ApJ, 575, 127
Hine R. G., Longair M. S., 1979, MNRAS, 188, 111
Iwasawa K. et al., 2012, A&A, 546, A84
Jarosik N. et al., 2011, ApJS, 192, 14
Jia J., Ptak A., Heckman T., Zakamska N. L., 2013, ApJ, 777, 27
Kalberla P. M. W. et al., 2005, A&A, 440, 775
Kataoka J. et al., 2011, ApJ, 740, 29

Kim M., Ho L. C., Peng C. Y., Barth A. J., Im M., Martini P., Nelson C. H., 2008, ApJ, 687, 767
Krivonos R., Tsygankov S., Revnivtsev M., Grebenev S., Churazov E., Sunyaev R., 2010, A&A, 523, A61
Krivonos R., Tsygankov S., Lutovinov A., Revnivtsev M., Churazov E., Sunyaev R., 2012, A&A, 545, A27
La Franca F. et al., 2005, ApJ, 635, 864
Landi R., Bassani L., Malizia A., Stephen J. B., Bazzano A., Fiocchi M., Bird A. J., 2010, MNRAS, 403, 945
Lara L. et al., 2001, A&A, 378, 826
Lawrence A., 1991, MNRAS, 252, 586
Lister M. L., Gower A. C., Hutchings J. B., 1994, AJ, 108, 821
Liu Y., Jiang D. R., Gu M. F., 2006, ApJ, 637, 669
McLure R. J., Jarvis M. J., Targett T. A., Dunlop J. S., Best P. N., 2006, MNRAS, 368, 1395
Malizia A. et al., 2007, ApJ, 668, 81
Malizia A., Stephen J. B., Bassani L., Bird A. J., Panessa F., Ubertini P., 2009, MNRAS, 399, 944
Malizia A., Bassani L., Bazzano A., Bird A. J., Masetti N., Panessa F., Stephen J. B., Ubertini P., 2012, MNRAS, 426, 1750
Malizia A., Molina M., Bassani L., Stephen J. B., Bazzano A., Ubertini P., Bird A. J., 2014, ApJ, 782, L25
Malizia A., Landi R., Molina M., Bassani L., Bazzano A., Bird A. J., Ubertini P., 2016, MNRAS, 460, 19
Marchesini D., Celotti A., Ferrarese L., 2004, MNRAS, 351, 733
Masetti N. et al., 2013, A&A, 556, A120
Matt G., Bianchi S., Guainazzi M., Barcons X., Panessa F., 2012, A&A, 540, A111
Mauch T., Murphy T., Buttery H. J., Curran J., Hunstead R. W., Piestrzynski B., Robertson J. G., Sadler E. M., 2003, MNRAS, 342, 1117
Mereminskiy I. A., Krivonos R. A., Lutovinov A. A., Sazonov S. Yu., Revnivtsev M. G., Sunyaev R. A., 2016, MNRAS, 459, 140
Mezcua M., Lobanov A. P., Chavushyan V. H., León-Tavares J., 2011, A&A, 527, A38
Miller B. P., Brandt W. N., 2009, ApJ, 695, 755
Mingo B., Hardcastle M. J., Croston J. H., Dicken D., Evans D. A., Morganti R., Tadhunter C., 2014, MNRAS, 440, 269
Molina M. et al., 2007, MNRAS, 382, 937
Molina M., Bassani L., Malizia A., Bird A. J., Bazzano A., Ubertini P., Venturi T., 2014, A&A, 565, A2
Molina M., Venturi T., Malizia A., Bassani L., Dallacasa D., Lal D. Vir, Bird A. J., Ubertini P., 2015, MNRAS, 451, 2370
Morganti R., Killeen N. E. B., Tadhunter C. N., 1993, MNRAS, 263, 1023
Morganti R., Oosterloo T., Tadhunter C. N., Aiudi R., Jones P., Villar-Martin M., 1999, A&AS, 140, 355
Osterbrock D. E., 1981, ApJ, 249, 462
Owen F. N., Laing R. A., 1989, MNRAS, 238, 357
Page K. L., Schartel N., Turner M. J. L., O'Brien P. T., 2004, MNRAS, 352, 523
Panessa F., Bassani L., 2002, A&A, 394, 435
Panessa F., Bassani L., Cappi M., Dadina M., Barcons X., Carrera F. J., Ho L. C., Iwasawa K., 2006, A&A, 455, 173
Prandoni I., Seymour N., 2015, Advancing Astrophysics with the Square Kilometre Array (AASKA14), p. 67, Available at http://pos.sissa.it/cgi-bin/reader/conf.cgi?
Reid R. I., Kronberg P. P., Perley R. A., 1999, ApJS, 124, 285
Reynolds C. S. et al., 2015, ApJ, 808, 154
Risaliti G., Maiolino R., Salvati M., 1999, ApJ, 522, 157
Rottgering H. J. A., Tang Y., Bremer M. A. R., de Bruyn A. G., Miley G. K., Rengelink R. B., Bremer M. N., 1996, MNRAS, 282, 1033
Runnoe J. C., Brotherton M. S., Shang Z., DiPompeo M. A., 2013, MNRAS, 434, 848
Sadoun R., Colin J., 2012, MNRAS, 426, L51
Sambruna R. M., Eracleous M., Mushotzky R. F., 1999, ApJ, 526, 60
Sambruna R. M., Reeves J. N., Braito V., 2007, ApJ, 665, 1030
Sazonov S., Revnivtsev M., Krivonos R., Churazov E., Sunyaev R., 2007, A&A, 462, 57
Sazonov S., Krivonos R., Revnivtsev M., Churazov E., Sunyaev R., 2008, A&A, 482, 517
Sazonov S., Churazov E., Krivonos R., 2015, MNRAS, 454, 1202
Sbarrato T., Ghisellini G., Maraschi L., Colpi M., 2012, MNRAS, 421, 1764
Schoenmakers A. P., Mack K.-H., Lara L., Röttgering H. J. A., de Bruyn A. G., van der Laan H., Giovannini G., 1998, A&A, 336, 455
Siemiginowska A., LaMassa S., Aldcroft T. L., Bechtold J., Elvis M., 2008, ApJ, 684, 811
Slee O. B., Sadler E. M., Reynolds J. E., Ekers R. D., 1994, MNRAS, 269, 928
Sobolewska M. A., Siemiginowska A., Migliori G., Stawarz Ł., Jamrozy M., Evans D., Cheung C. C., 2012, ApJ, 758, 90
Tadhunter C., Marconi A., Axon D., Wills K., Robinson T. G., Jackson N., 2003, MNRAS, 342, 861
Tazaki F., Ueda Y., Ishino Y., Eguchi S., Isobe N., Terashima Y., Mushotzky R. F., 2010, ApJ, 721, 1340
Tazaki F., Ueda Y., Terashima Y., Mushotzky R. F., Tombesi F., 2013, ApJ, 772, 38
Tombesi F., Tazaki F., Mushotzky R. F., Ueda Y., Cappi M., Gofford J., Reeves J. N., Guainazzi M., 2014, MNRAS, 443, 2154
Torresi E., Grandi P., Guainazzi M., Palumbo G. G. C., Ponti G., Bianchi S., 2009, A&A, 498, 61
Torresi E., Grandi P., Costantini E., Palumbo G. G. C., 2012, MNRAS, 419, 321
Treister E., Urry C. M., 2006, ApJ, 652, L79
Trippe M. L., Crenshaw D. M., Deo R. P., Dietrich M., Kraemer S. B., Rafter S. E., Turner T. J., 2010, ApJ, 725, 1749
Ueda Y., Akiyama M., Ohta K., Miyaji T., 2003, ApJ, 598, 886
Ueda Y. et al., 2007, ApJ, 664, L79
Ueda Y., Akiyama M., Hasinger G., Miyaji T., Watson M. G., 2014, ApJ, 786, 104
Urry C. M., Padovani P., 1995, PASP, 107, 803
Vasudevan R. V., Fabian A. C., 2007, MNRAS, 381, 1235
Vasudevan R. V., Mushotzky R. F., Gandhi P., 2013, ApJ, 770, L37
Vignali C., Mignoli M., Gilli R., Comastri A., Iwasawa K., Zamorani G., Mainieri V., Bongiorno A., 2014, A&A, 571, A34
Wandel A., 2002, ApJ, 565, 762
Wang J., Mao Y. F., Wei J. Y., 2009, AJ, 137, 3388
Wilkes B. J. et al., 2013, ApJ, 773, 15
Wilman R. J., Edge A. C., Johnstone R. M., 2005, MNRAS, 359, 755
Winter L. M., Mushotzky R. F., Tueller J., Markwardt C., 2008, ApJ, 674, 686
Winter L. M., Lewis K. T., Koss M., Veilleux S., Keeney B., Mushotzky R. F., 2010, ApJ, 710, 503
Woo J.-H., Urry C. M., 2002, ApJ, 579, 530
Wu Q., 2009, MNRAS, 398, 1905
Wu X.-B., Liu F. K., 2004, ApJ, 614, 91

APPENDIX A: *Swift*/XRT DATA REDUCTION AND ANALYSIS

We took all radio galaxies from the sample of Bassani et al. (2016) and extracted 13 objects for which X-ray spectral information was not found in the literature. This list of sources was then cross-correlated with the *Swift*/XRT archival data set, and for all sources we found X-ray observations available in the archive. The log of all X-ray observations analysed in this work is given in Table A1, where we report for each individual radio galaxy the XRT observation ID, the date and the exposure of the XRT pointings.

The XRT data were processed using the XRTDAS standard data pipeline package (XRTPIPELINE v. 0.12.9) to produce calibrated and cleaned PC-mode event file. Observations were summed together using XSELECT v. 2.4c. XRT images in the 0.3–10 keV energy band were obtained and analysed by means of the software package XIMAGE v. 4.5.1. We found that all sources were detected by XRT, although not all with good statistical significance.

Table A1. Log of the *Swift*/XRT observations used in this paper.

Source name	ID	Obs date	Exposure (s)
PKS 0018−19	00040886001	Sep 27, 2010	8037
	00040691001	Jan 30, 2011	6494
total obs	–	–	14 531
PKS 0101−649	00047109001	Nov 01, 2011	864
	00047109002	Nov 11, 2011	2778
	00047109003	Nov 17, 2011	166
	00047109004	Nov 20, 2011	241
	00047109005	Nov 23, 2011	637
	00047109006	Nov 25, 2011	2641
	00047109007	Apr 05, 2012	2101
total obs	–	–	9428
4C +10.08	00037347001	Dec 05, 2010	527
	00037347002	Dec 14, 2010	6956
	00037347003	Mar 02, 2011	1143
	00037347004	Mar 06, 2011	2061
total obs			10 687
B3 0749+460A	00037357001	Feb 24, 2008	9353
2MASX J14364961−1613410	00040978001	Dec 25, 2010	595
	00040978002	Apr 12, 2011	222
	00047122001	Apr 12, 2012	193
	00047122003	May 08, 2013	632
	00047122004	May 10, 2013	110
	00047122005	May 20, 2013	865
	00047122006	May 21, 2013	2775
	00047122007	May 26, 2013	341
	00047122008	May 27, 2013	3874
total obs			9607
4C +63.22	00035401002	Oct 17, 2006	5546
4C +23.42	00038073001	Sep 25, 2008	2269
	00038073002	Sep 26, 2008	4930
	00038073004	Jan 04, 2009	6690
total obs			13 889
LEDA 100168	00037998001	Jul 05, 2008	4885
	00037998002	Jul 06, 2008	2563
	00037998002	Jul 06, 2008	2563
	00037998002	Jul 07, 2008	2532
total obs			9980
PKS 1737−60	00047123001	Nov 10, 2011	836
	00047123002	Nov 11, 2011	5204
	00047123003	Nov 14, 2011	1123
	00047123004	Nov 17, 2011	2871
total obs			10 034
4C +18.51	00041782001	Oct 31, 2010	2490
	00041782002	Jan 13, 2011	1586
	00041782003	Jan 21, 2011	1715
	00041782004	Jan 25, 2011	1680
	00041782004	Jan 28, 2011	3003
total obs			10 474
2MASX J22194971+2613277	00041122002	Jul 12, 2010	3181
	00041122003	Jul 13, 2010	7165
	00041122004	Jul 15, 2010	946
	00041122005	Jul 17, 2010	1991
total obs			13 283
PKS 2331−240	00031731001	Jun 05, 2010	1668
	00031731002	Jun 05, 2010	3924
	00041128001	Sep 29, 2010	9052
total obs			14 644

For the spectral analysis, source events were extracted within a circular region with a radius of 20 pixels (1 pixel ∼2.36 arcsec) centred on the source position, while background events were extracted from a source-free region close to the X-ray source of interest. The spectra were obtained from the corresponding event files using the XSELECT V. 2.4C software and binned using GRPPHA in an appropriate way, so that the χ^2 statistic could be applied. We used version v.014 of the response matrices and created individual ancillary response files *arf* using XRTMKARF V. 0.6.0.

Next, we combined the XRT spectra with the BAT ones (from the 70-month BAT catalogue; Baumgartner et al. 2013)[5] to perform the spectral analysis over the 0.3–100 keV energy range. We adopted a simple absorbed power-law model to fit the source spectra where absorption is partly due to a Galactic column density in the source direction (fixed value) and partly due to an intrinsic column density (free parameter). We also introduced in the fitting procedure a cross-calibration constant ($C_{\rm calib}$) to account for a possible mismatch between XRT and BAT data, as well as for source flux variations.

The results of the spectral fittings are shown in Table A2 where we report for each source the value of the Galactic column density, the photon index, the 2–10 keV luminosity, the χ^2/ν values of the fit and the XRT/BAT cross-correlation constant, while intrinsic absorption values, as well as 2–10 keV fluxes, are given in Table 1 of the main text. In the fitting procedure, when no absorption is measured, the Galactic column density value is used as an upper limit to the amount of absorption.

Those sources for which this simple model does not fit the data properly, indicating the need for an extra feature, are briefly discussed as follows.

4C +63.22. For this source, our baseline model does not provide a good fit to the data ($\chi^2/\nu = 69.0/43$) as residuals, indicative of an absorbing feature at around 0.9 keV, are clearly visible in the data-to-model ratio. We therefore tested our data for the presence of an absorption edge, leaving all the parameters free to vary: the fit improves significantly ($\chi^2/\nu = 38.4/41$) and the component is required by the data at more than 99.99 per cent confidence level. The absorption edge turned out to be at 0.94 ± 0.06 and have $\tau_{\rm max} = 0.91^{+0.34}_{-0.30}$, thus indicating an origin from Fe XX. This result is not surprising as Molina et al. (2015) have recently detected absorption features from ionized elements in the giant radio galaxy IGR J14488−4008.

PKS 2014−55. This is another case in which the baseline model does not provide a good fit to the data ($\chi^2/\nu = 35.8/12$) as an excess below 1 keV is observed in the residuals. Also in this case we added to the baseline model a second power law passing through intrinsic absorption, having the same photon index of the primary one, which yields an improvement (> 99.99 per cent) of the fit as shown in Table A2.

PKS 2300−18. For this source, there is a hint of an excess around 6 keV, again due to neutral iron, which we modelled by adding a narrow-line component. This feature is required at around 99.8 per cent ($\Delta\chi^2/\nu = 14.6/2$) and provides a line centroid at 6.51 ± 0.10 and an EW $= 608^{+267}_{-272}$ eV.

[5] Available at http://swift.gsfc.nasa.gov/results/bs70mon/.

Table A2. XRT spectral analysis results.

Source name	$N_{H(Gal)}^{a}$	Γ	L(2–10 keV)^{b}	χ^2/ν	C_{calib}^{c}	Model
PKS 0018−19	0.0201	1.72 ± 0.12	2.37	105.5/109	$0.55^{+0.22}_{-0.16}$	absorbed pl
PKS 0101−649	0.0231	1.69 ± 0.09	2.16	33.8/48	$1.00^{+0.47}_{-0.34}$	simple pl
4C +10.08	0.100	$1.70^{+0.31}_{-0.29}$	0.262	17.7/21	$1.78^{+2.00}_{-0.99}$	absorbed pl
B3 0749+460A	0.0179	1.64 ± 0.08	0.188	61.9/49	$1.22^{+0.48}_{-0.36}$	simple pl
2MASX J14364961−1613410	0.0759	1.72 ± 0.06	3.90	74.5/93	$0.79^{+0.29}_{-0.23}$	simple pl
4C +63.22	0.0148	1.96 ± 0.08	4.30	38.4/41	$1.38^{+0.63}_{-0.46}$	simple pl + absorption edge
4C +23.42	0.0416	1.67 ± 0.21	1.11	46.3/38	$1.07^{+0.91}_{-0.50}$	absorbed pl
LEDA 100168	0.0593	1.75 ± 0.11	3.91	67.4/65	$0.97^{+0.45}_{-0.31}$	absorbed pl
PKS 1737−60	0.0584	1.94 ± 0.07	23.3	86.1/75	$1.55^{+0.72}_{-0.56}$	simple pl
4C +18.51	0.0551	1.83 ± 0.07	4.72	66.3/75	$0.81^{+0.41}_{-0.33}$	simple pl
PKS 2014−55	0.0481	1.86 ± 0.21	0.304	17.2/10	$1.01^{+0.72}_{-0.42}$	double pl
2MASX J22194971+2613277	0.0664	1.69 ± 0.11	1.18	70.1/85	$0.73^{+0.31}_{-0.22}$	absorbed pl
PKS 2300−18	0.0217	1.83 ± 0.21	2.24	139.0/117	$1.01^{+0.39}_{-0.33}$	simple pl + iron line
PKS 2331−240	0.0163	1.70 ± 0.04	0.375	147.5/138	$0.60^{+0.18}_{-0.16}$	simple pl

Notes. [a]In units of 10^{22} cm^{-2} (from Kalberla et al. 2005).
[b]In units of 10^{44} erg s^{-1}.
[c]IBIS/XRT cross-calibration constant.

This paper has been typeset from a TEX/LATEX file prepared by the author.